
ICE VISCOSITY IS MORE SENSITIVE TO STRESS THAN COMMONLY ASSUMED

Joanna D. Millstein^{1*}, Brent M. Minchew², Samuel S. Pegler³

¹Massachusetts Institute of Technology - Woods Hole Oceanographic Institute Joint Program in
Oceanography/Applied Ocean Science and Engineering, Cambridge, MA, USA

²Department of Earth, Atmospheric, and Planetary Sciences, Massachusetts Institute of Technology,
Cambridge, MA, USA

³School of Mathematics, University of Leeds, Leeds, UK

*To whom correspondence should be addressed; E-mail: jdmill@mit.edu.

Preprint, compiled February 14, 2021

Accepted at *Nature Communications Earth & Environment*.

ABSTRACT

1 Accurate representation of the viscous flow of ice is fundamental to understanding glacier dynamics
2 and projecting sea-level rise. Ice viscosity is often described by a simple but largely untested and
3 uncalibrated constitutive relation, Glen's Flow Law, wherein the rate of deformation is proportional
4 to stress raised to the power n . The value $n = 3$ is commonly prescribed in ice-flow models, though
5 observations and experiments support a range of values across stresses and temperatures found on
6 Earth. Here, we leverage recent remotely-sensed observations of Antarctic ice shelves to show that
7 Glen's Flow Law approximates the viscous flow of ice with $n = 4.1 \pm 0.4$ in fast-flowing areas. The
8 viscosity and flow rate of ice are therefore more sensitive to changes in stress than most ice-flow
9 models allow. By calibrating the governing equation of ice deformation, our result is a pathway
10 towards improving projections of future glacier change.

11 Introduction

12 Mass loss from ice sheets presents both the greatest potential contribution to future sea-level rise and the largest source
13 of uncertainty in such estimates^{1,2}. In Antarctica, mass loss occurs principally through fast-flowing glaciers that flow
14 into floating ice shelves, which provide resistive buttressing stresses that impede the seaward flow of ice and stabilize
15 marine grounding zones³⁻⁵. The rate at which glaciers flow is controlled by the shear-thinning viscous deformation
16 of ice⁶. The most commonly adopted constitutive relation, known as Glen's Flow Law, is often employed to quantify
17 the viscous deformation of glacier ice by relating the rate of deformation, hereafter called strain rate, to the deviatoric
18 stress⁷. Glen's Flow Law is most simply expressed as

$$\dot{\epsilon}_e = A\tau_e^n \quad (1)$$

19 where $\dot{\epsilon}_e$ is the effective strain rate, τ_e the effective deviatoric stress, n the stress exponent, and A the rate factor or
20 flow-law coefficient. Variation in the parameter A can be used to represent the effects of temperature, grain size, grain
21 orientation (fabric), impurities, and interstitial water content⁸.

22 Glen's Flow Law is routinely implemented in large-scale ice-flow models with the prescribed value $n = 3$ assumed to
23 be constant in space and time^{9,10}. Glen's laboratory experiments pinpointed the power-law rheology and extrapolated
24 his findings to flows of natural ice^{7,8,11}. Shortly thereafter, Glen's findings and supporting evidence were widely adopted
25 in the glaciological literature, with the field converging on the canonical value of $n = 3$ ¹²⁻¹⁴. However, multiple
26 mechanisms influence the viscous deformation of ice, each with a suggested value of n : dislocation creep ($n = 4$),
27 grain-boundary sliding ($n \approx 2$, with slight variance dictated by the direction of motion of dislocations), and diffusion
28 creep ($n = 1$) all accommodate creep at the individual grain level and, in aggregate, describe the flow of glacier
29 ice¹⁵. These mechanisms are not treated independently in Glen's Flow Law (Eq. 1). Rather, it serves as a lumped
30 parameterization representing the combined effect of all mechanisms. Generalized forms of the flow law have been

31 proposed to account for multiple creep mechanisms, fabric, and grain size, but these have not been widely tested,
 32 calibrated, nor implemented^{10,15,16}.

33 The simplicity of Glen’s Flow Law has proven useful and, subject to suitable calibration under different conditions,
 34 has the potential to provide a reasonably accurate general description of the flow of glacier ice^{7,8,14,17}. Glen’s Flow
 35 Law (Eq. 1) with $n = 3$ shows consistency with sparse observations of natural ice flows such as borehole deformation
 36 measurements and ice flow velocities, as well as laboratory experiments on polycrystalline ice aggregates under
 37 conditions relevant for ice sheets^{7,15,18–25}. However, the broad range of conditions over which the rheological behavior
 38 of ice has been examined reveals the way in which variations in stress can influence the stress exponent and, in turn, the
 39 mechanisms of creep^{10,26–28}. Nearly 70 years after its introduction, the need remains to test and rigorously calibrate the
 40 parameters n and A in the natural environment.

41 We infer the stress exponent of Glen’s Flow Law across wide areas of Antarctic ice shelves, the floating extensions
 42 of the ice sheet. Using satellite observations, we are able to address the long-standing problem of benchmarking a
 43 flow law that can be used in ice-flow models. The abundance and extent of the data allows us to investigate the creep
 44 of glacial ice on a continental scale, assembling inferences to reveal spatial coherence and patterns with statistical
 45 constraints. To do so, we require independent estimates of strain rates and (deviatoric) stresses (Eq. 1). The schematic
 46 in Figure 1 graphically illustrates the methodology, showing how we begin with independent observations of surface
 47 velocities and ice thicknesses, apply these to evaluate strain-rates $\dot{\epsilon}_e$ and stresses τ_e , and then conduct a regression
 48 analysis to infer the parameters in Glen’s Flow Law. This method is comparable to previously published work^{21,22,26,29},
 49 but applied to Antarctic ice shelves using continental-scale remote sensing observations. Our results reveal that a
 50 value of $n = 4.1 \pm 0.4$ is the most representative flow law exponent in fast-flowing, extensional regions, where the
 51 magnitude of deviatoric stresses are comparable to those expected in other dynamic regions of the ice sheet. Making
 52 use of continent-scale remote sensing observations on Antarctic ice shelves, we demonstrate how the viability of a
 53 power-law rheology can be constrained directly using observations.

54 We focus on ice shelves because the underlying ocean provides negligible shear resistance to ice flow, allowing for
 55 two important simplifications in our analysis. First, we can neglect drag at the base of the ice and thus consider a
 56 stress regime that is simpler for our purposes than would be expected for grounded ice, where basal drag presents a
 57 further unknown that must be constrained. Second, the lack of drag at the base means that strain rates are approximately
 58 constant with depth. For this reason, the horizontal strain rates we calculate from observations of the surface velocity
 59 fields approximate the strain rates at all depths.

60 Ice shelves cover areas that are large compared with the sub-kilometer resolution of observations, providing ample
 61 opportunities to comprehensively observe broad regions of flow undergoing relatively simple one-dimensional deforma-
 62 tion. As a result, we can focus on regions that are close to being in pure extension, where the ice spreads under its own
 63 weight in one direction and the governing equations of flow reduce to a simple two-term balance, detailed further in this
 64 report. This basic premise has been employed for decades to study the rheology of glacier ice^{22,24,30} but has not been
 65 systematically applied on continental scales before now.

66 We use measurements of ice thickness provided through the BedMachine project³¹, and surface velocity data from
 67 the NASA Inter-mission Time Series of Land Ice Velocity and Elevation (ITS_LIVE) project³². The surface velocity
 68 data, which encompass most of the Antarctic Ice Sheet at a grid spacing of $120 \text{ m} \times 120 \text{ m}$, are derived from Landsat
 69 4, 5, 7, and 8 imagery using the auto-RIFT feature tracking processing chain, providing reliable constraints on the
 70 two horizontal components of ice velocity³². We use these to calculate the horizontal strain rates $\dot{\epsilon}_{ij}$ (for $i, j = x, y$
 71 the two horizontal coordinates) across all Antarctic ice shelves, as defined by $2\dot{\epsilon}_{ij} = (\partial u_i / \partial x_j + \partial u_j / \partial x_i)$, where
 72 u_i represents the horizontal components of the ice velocity vector and x_i the horizontal coordinates. To calculate the
 73 components of the velocity gradient, we apply a two-dimensional Savitzky-Golay filter with a polynomial order of one
 74 and square window of 3720 m (31 pixels)³³. More detail on the strain rate calculations are found in the Supplementary
 75 Methods.

76 After deriving strain rates from the surface velocity fields, we determine regions flowing in approximately pure extension,
 77 with a view to simplifying the force balance governing the local ice flow. The two-dimensional strain rate tensor $\dot{\epsilon}_{ij}$ has
 78 three unique components (the off-diagonal terms are equal by definition) and a scalar invariant representing the effective
 79 horizontal strain rate $\dot{\epsilon} = \sqrt{\dot{\epsilon}_{ij}\dot{\epsilon}_{ij}/2}$, where summation is implied for repeated indices. Note that the effective strain
 80 rate $\dot{\epsilon}_e$ in Eq. 1 follows the same definition as for $\dot{\epsilon}$ but is applied to the three-dimensional strain-rate tensor. We focus
 81 on areas of the ice shelves that are solely confined by seaward pressure in the along-flow, or x , direction, and analyze
 82 areas in which the along-flow component of the strain rate tensor $\dot{\epsilon}_{xx}$ is much larger than both lateral normal and shear
 83 strain rates ($\dot{\epsilon}_{xx} \gg \dot{\epsilon}_{yy}, \dot{\epsilon}_{xy}$). We combine these into the single criterion $\dot{\epsilon}_{xx} \approx \sqrt{2}\dot{\epsilon}$, corresponding to areas of the ice
 84 shelves where longitudinal extension is dominant. The more specific criterion $\dot{\epsilon}_{xx} > \dot{\epsilon}$ is used to define large, spatially
 85 coherent regions where the extensional component of deformation dominates the flow (Fig. 2 and Supplementary
 86 Figures S1 and S2). Approximately 20% of the total surface area of all Antarctic ice shelves satisfies this criterion. In

87 these areas it follows from the incompressibility of ice and the absence of drag at the base of ice shelves that $\dot{\epsilon}_{xx} \approx \dot{\epsilon}_e$,
 88 the three-dimensional effective strain rate in Eq. 1.

89 To estimate the effective deviatoric stress from remote sensing observations, we utilize a well-established reduced form
 90 of the Stokes equations that govern the viscous flow of glacier ice. Over the ice shelves, where negligible shear stress
 91 applies at both the upper (atmosphere) and lower (ocean) surfaces of the ice, we can adopt the depth-integrated form
 92 of the Stokes equations commonly referred to as the Shallow-Shelf Approximation (SSA), which contains only body
 93 forces and the horizontal gradients of the stress tensor elements. Based on the conditions described above, we can
 94 further reduce the SSA equations to a simple expression relating the (depth-averaged) along-flow deviatoric stress τ_{xx}
 95 to local ice thickness H as:

$$\tau_{xx} = \rho g' H/4 \quad (2)$$

96 where $g' = g(1 - \rho/\rho_w)$ is the reduced gravity, representing the balance between the resistive longitudinal stress and
 97 the driving buoyancy force (the full derivation is provided in the Methods). Here, we take $\rho = 910 \text{ kg/m}^3$ as the mass
 98 density of glacier ice and $\rho_w = 1026 \text{ kg/m}^3$ as the mass density of seawater. Where the criteria for predominantly
 99 extensional flow is met ($\dot{\epsilon}_{xx} \approx \dot{\epsilon}_e$), we expect $\tau_{xx} \approx \tau_e$. Thus, the criteria we apply to the strain rate fields to identify
 100 areas in primarily extensional flow allows us to calculate effective stress τ_e (Eq. 1) from observations of ice thickness
 101 and independently of the surface velocity fields used to calculate $\dot{\epsilon}_e$. Before fitting a model to the data, we ensure that
 102 the gradients of horizontal shear stress transverse to flow are small compared to the gradients of longitudinal stress from
 103 the position of the ice parcel all the way to the ice shelf calving front. This supports the suitability of the derivation for
 104 effective stress over the fast-flowing, extensional regions of Antarctic ice shelves of interest.

105 Critically, this study does not take into account firn or marine ice, which are characteristic of all ice shelves, nor do
 106 we need to explicitly account for viscous anisotropy (fabric). Complexities caused by firn and marine ice are partially
 107 subsumed by the uniform density profile but remain a source of uncertainty in our analysis. Given that the mass densities
 108 of firn and ice are within a factor of two and firn typically comprises a thin upper layer of ice shelves, we expect the
 109 uncertainties due to firn and marine ice are small enough to not meaningfully impact our results. Our focus on a single
 110 flow regime and parcels of ice defined along and parallel to flow lines allow us to avoid the complexities that arise from
 111 viscous anisotropy in ice, which would require a non-scalar form of A to represent deformation in multiple directions,
 112 and spatial variations in characteristics like ice temperature and liquid water content.

113 Results

114 Linear regressions fitted to the values for $\log(\dot{\epsilon}_e)$ and $\log(\tau_e)$ constrain n through the slope and A in the y -intercept,
 115 divulging values of the flow law parameters across viable regions of Antarctic ice shelves. To determine 95% confidence
 116 intervals on the regression of strain rate on stress, we implement a non-parametric bootstrap which allows us to estimate
 117 constraints on the determined value of n without making assumptions on the underlying structure of the distribution³⁴.
 118 Our analysis encompasses regions of both large ice shelves, such as those shown in Figure 2, and smaller ice shelves
 119 that line the continent. We focus first on highlighted areas on the Ross and Filchner-Ronne Ice Shelves in Figure 2,
 120 which we extracted from areas along flow lines, with probable consistency between values of temperature, grain size,
 121 and fabric, and therefore A and n .

122 The log-log plots between strain rate and deviatoric stress shown in Figure 2 exhibit linear trends that are consistent
 123 with a power-law relation. These results provide strong evidence that, for a suitable choice of n , Glen's Flow Law is a
 124 viable approximation of the viscous flow of Antarctic ice shelves and, as discussed later, likely other dynamic regions
 125 of Antarctica. Critically, we find $n \approx 4$ in the fast-flowing, extensional regions of Antarctic ice shelves. This result is
 126 consistent with other evidence for a higher value of the flow law exponent^{7,24,26,30,35,36}, and demonstrates that this higher
 127 value is applicable to natural ice flow at the continental scale. Additional comparison with the value $n = 3$ and other
 128 typical values of the existing flow law can be found in Supplementary Figure S3; it is worth noting that $n = 3$ provides
 129 a poor fit to the data used in this study as shown in Figure 2. Additionally, the residuals from the linear regressions in
 130 subplots a-h of Figure 2 are shown in Supplementary Figure S4 and demonstrate the suitability of the linear fit in these
 131 areas.

132 The results of our full analysis covering all viable regions of Antarctic ice shelves is shown in Figure 3, which includes
 133 regions of both large and small ice shelves (mapped in Supplementary Figures S1 and S2). The normalized kernel
 134 density estimates of the bootstrapped values of the flow law exponent (Figure 3) indicate that $n = 4.1 \pm 0.4$ in
 135 extensional regions of Antarctic ice shelves. Figure 3 shows the confidence with which our estimate stands across
 136 geographic areas of different sizes and representing a range of stresses. Large areas extracted for analysis, $> 1000 \text{ km}^2$,
 137 have less spread in the error estimation and are centered closer to $n = 4.1$, whereas smaller areas exhibit a greater
 138 spread in the distribution. This is likely because the broader ranges of stresses and greater number of observations
 139 in the larger ice shelves provide more accurate inferred trends across the data. Notably, geographic regions from

140 West Antarctica have slightly higher values of n than regions sampled from East Antarctica. This observation could
 141 be attributed to higher sub-ice-shelf melt rates in West Antarctic ice shelves, where the bulk of ice is created on the
 142 ice shelf by compaction of snow as opposed to being inherited from the grounded glacier³⁷. Additionally, there is a
 143 possible grain size dependence wherein warmer conditions would contribute to larger grains^{38,39}. In such regions, larger
 144 grains, strain rate, and values of the stress exponent validate a hypothesis that ice deformation is facilitated primarily by
 145 dislocation creep^{15,29}. Our results highlight further spatial variability in the precise values of the flow law exponent and
 146 rate factor across different ice shelves, and even different regions within single ice shelves (see Figure 3). We reserve
 147 for future work detailed analysis and modeling of these variations.

148 We find values of the flow law rate factor, A , spanning 10^{-35} to 10^{-27} Pa $^{-n}$ s $^{-1}$ for the range of inferred n values (see
 149 Supplement Figure S5). Inferred values of A depend on the inferred values of n . Here, we do not attempt to provide
 150 newly calibrated values for A because proper constraints on the physical properties of the ice, like temperature and
 151 grain size, are not currently available in these areas and require work that is beyond the scope of this study. Rather, we
 152 note that the smaller values of A found here validate our method for deriving Glen's Flow Law and we recommend that
 153 future efforts using a value $n \approx 4$ utilize standard tabulated sources for A ⁴⁰ and scale these values accordingly for the
 154 new value of n . A comparison of our results to the more commonly used $n = 3$ can be seen in Supplement Figure S3,
 155 highlighting the incompatible values of A in these results, and the generally poor fit of $n = 3$ to the data.

156 Conclusion

157 The result that $n \approx 4$ challenges the long-held practice of assuming the flow law exponent is $n = 3$ everywhere, and at
 158 all times, in large-scale ice-sheet flow models. While our observations focus on specific regions in extensional flow
 159 regimes on ice shelves that experience stresses of order 100 kPa (Supplement Figure S6), complementary laboratory
 160 work showing that $n = 4$ is suitable at higher stresses¹⁵ supports extending our conclusion that $n \approx 4$ to other dynamic
 161 regions in Antarctica. Additionally, our conclusion complements a growing body of work advocating for the use of
 162 $n > 3$ in other areas of the cryosphere^{19,26}. Taken together, this work calls for a broader community effort to quantify
 163 the uncertainties in the flow-law parameters and the consequences of these uncertainties on models of glacier dynamics.
 164 A higher value of n increases the sensitivity of viscosity to changes in stress but the impact of $n = 4$ on large-scale
 165 ice-flow models used for projections of sea-level rise and ice-sheet evolution remains unclear as few sensitivity analyses
 166 have been conducted¹⁰ and n is not a parameter explored in current ensemble-model analyses^{1,2}. The value $n = 4$ has
 167 the potential to increase the sensitivity of ice-sheet mass loss to ongoing climate change considerably relative to $n = 3$
 168 due to the stronger dependence of flow rates to changes in resistive stresses.

169 By applying continental-scale satellite observations to standard models in glacier dynamics, we have validated Glen's
 170 Flow Law, a constitutive relationship that helps form the foundation of modern glaciology, and calibrated the stress
 171 exponent in Antarctic ice shelves. This work serves as a pathway towards a standard calibration framework for the
 172 community using publicly available remote sensing data. Our conclusion that $n \approx 4$ across much of Antarctica's ice
 173 shelves is a step towards reassessing the governing equations of ice flow in the satellite age, and reveals an increased
 174 sensitivity of flow rates to applied stresses relative to the commonly used $n = 3$. As a consequence, future sea-level rise
 175 is likely more sensitive to climate forcings than predicted by present models using common assumptions of the flow law.

176 Methods

177 Solving for Effective Stress

178 Conservation of momentum (Stokes equations) describes all forces acting on the volume of glacier ice such that

$$\frac{\partial \tau_{ij}}{\partial x_j} - \frac{\partial p}{\partial x_i} - \rho g_i = 0 \quad (3)$$

179 where p is the pressure, ρg_i is the driving gravitational force (with $\mathbf{g} = g\hat{z}$), and summation is implied for repeated
 180 indices. For a layer of ice floating on top of an ocean, we can derive depth-integrated equations to describe the balance
 181 of forces in such a system, given that the ice shelf is much larger in horizontal extent than in thickness⁴¹. At scales
 182 of order the ice thickness, bending (and bridging) stresses are negligible, allowing us to simplify the equilibrium
 183 equations⁴². As a result, we take the vertical normal stress to be equivalent to the overburden stress (weight of the ice
 184 per unit area). This can be expressed as

$$p = -\rho g z + \rho g' H + \tau_{zz} = -\rho g z + \rho g' H - \tau_{xx} - \tau_{yy} \quad (4)$$

185 where H is the ice thickness, $g' = g(\rho_w - \rho)/\rho_w$ is the reduced gravity, and the second equality arises from the fact
 186 that the deviatoric stress tensor is traceless. Eq. 4 is derived by integrating the vertical component of Eq. 3 and applying
 187 the condition of continuous normal stress at the top and bottom of the layer.

188 Then, neglecting basal drag (due to our focus on ice shelves) and depth integrating the x -component of Eq. 3, we can
 189 obtain

$$\frac{\partial}{\partial x} [H(2\tau_{xx} + \tau_{yy})] + \frac{\partial}{\partial y} (H\tau_{xy}) = \rho g' H \frac{\partial H}{\partial x}. \quad (5)$$

190 where all deviatoric stresses are now depth-averaged. A complete derivation can be found in⁴³, which uses different
 191 notation but reveals the same outcome. A comparable derivation is found in³⁰ with the notable distinction here being
 192 our omission of $\alpha = \tau_{yy}/\tau_{xx}$ because we only consider areas where $\alpha \ll 1$. In this way, we are able to look at large
 193 areas without potential complications arising from multiple stress components (e.g. viscous anisotropy).

194 We can simplify Eq. 5 in two steps. First, we assume that the lateral normal stresses (τ_{yy}) are negligibly small compared
 195 with the longitudinal normal stresses (τ_{xx}) due to our emphasis on areas with $\dot{\epsilon}_{xx} \gg \dot{\epsilon}_{yy}$ ⁴⁴. Then, we apply the
 196 constitutive relation in Supplementary Eq. 6 and recall that in our areas of interest, we require that $\dot{\epsilon}_{xx} \approx \dot{\epsilon}_e$. Thus, Eq.
 197 5 becomes

$$2 \frac{\partial}{\partial x} (\phi) + \frac{\partial}{\partial y} (\beta\phi) = \rho g' H \frac{\partial H}{\partial x} \quad (6)$$

198 where $\phi = h\dot{\epsilon}_{xx}^{1/n} A^{-1/n}$ and $\beta = \dot{\epsilon}_{xy}/\dot{\epsilon}_{xx}$. The derived strain rate data indicate that in our areas of interest, the lateral
 199 ($\partial/\partial y$) and longitudinal ($\partial/\partial x$) gradients in $h\dot{\epsilon}_{xx}$ have the same order of magnitude. Assuming A and n vary slowly
 200 in space in our areas of interest, then $\partial\phi/\partial y$ is of order $\partial\phi/\partial x$, placing the emphasis on the term β . Our criteria that
 201 $\dot{\epsilon}_{xx} \approx \dot{\epsilon}_e$ requires that $\beta \ll 1$ everywhere in our areas of interest, which are wide enough that $\partial\beta/\partial y$ is negligibly
 202 small. This means that within the error in currently available data, we can assume that the lateral shear term (second on
 203 the left hand side of Eqs. 5 and 6) is negligible.

204 Vastly reduced, what began as four components - extension, lateral shear, basal drag, and buoyancy - now only requires
 205 terms for extension and buoyancy to illustrate the force balance of an unconfined ice shelf⁴⁴. Equation 5 is now

$$\frac{\partial}{\partial x} (2H\tau_{xx}) = \rho g' H \frac{\partial H}{\partial x}. \quad (7)$$

206 We can now rearrange the right-hand side of Equation 7 to an equivalent form

$$\frac{\partial}{\partial x} (2H\tau_{xx}) = \frac{1}{2} \rho g' \frac{\partial}{\partial x} (H^2). \quad (8)$$

207 Integrating this equation subject to the free stress condition at the front of the ice shelf and simplifying the resulting
 208 equation results in

$$\tau_{xx} = \frac{1}{4} \rho g' H, \quad (9)$$

209 which we use as the basis for our analysis of extensional deviatoric stress in floating ice shelves. This derivation shows
 210 how we can use the extensional deviatoric stress as the total effective stress in our regions of interest, allowing us to use
 211 a dataset of ice thickness to determine the stress in the system parameter.

212 Data availability

213 No new data were generated in this analysis; the strain rate fields were generated using velocity data from
 214 NASA ITS_LIVE (<https://its-live.jpl.nasa.gov/>). The MEaSURES ice thickness data is available at the NSIDC
 215 (<https://nsidc.org/data/nsidc-0756/versions/2>).

216 Code availability

217 The Python codes used to analyze the remote sensing datasets and prepare figures are available on Github
 218 (https://github.com/jdmillstein/n_equals_4).

219 **References**

- 220 1. DeConto, R. M. *et al.* The Paris Climate Agreement and future sea-level rise from Antarctica. *Nature* **593**, 83–89
221 (2021).
- 222 2. Edwards, T. L. *et al.* Projected land ice contributions to twenty-first-century sea level rise. *Nature* **593**, 74–82
223 (2021).
- 224 3. Gudmundsson, G., Krug, J., Durand, G., Favier, L. & Gagliardini, O. The stability of grounding lines on retrograde
225 slopes. *The Cryosphere* **6**, 1497–1505 (2012).
- 226 4. Haseloff, M. & Sergienko, O. V. The effect of buttressing on grounding line dynamics. *Journal of Glaciology* **64**,
227 417–431 (2018).
- 228 5. Pegler, S. S. Marine ice sheet dynamics: the impacts of ice-shelf buttressing. *Journal of Fluid Mechanics* **857**,
229 605–647 (2018).
- 230 6. Nye, J. F. The flow law of ice from measurements in glacier tunnels, laboratory experiments and the Jungfraufirn
231 borehole experiment. *Proceedings of the Royal Society of London. Series A. Mathematical and Physical Sciences*
232 **219**, 477–489 (1953).
- 233 7. Glen, J. W. The creep of polycrystalline ice. *Proceedings of the Royal Society of London. Series A. Mathematical*
234 *and Physical Sciences* **228**, 519–538 (1955).
- 235 8. Glen, J. W. The flow law of ice: A discussion of the assumptions made in glacier theory, their experimental
236 foundations and consequences. *IASH Publ* **47**, e183 (1958).
- 237 9. Larour, E., Seroussi, H., Morlighem, M. & Rignot, E. Continental scale, high order, high spatial resolution, ice
238 sheet modeling using the Ice Sheet System Model (ISSM). *Journal of Geophysical Research: Earth Surface* **117**
239 (2012).
- 240 10. Zeitz, M., Levermann, A. & Winkelmann, R. Sensitivity of ice loss to uncertainty in flow law parameters in an
241 idealized one-dimensional geometry. *The Cryosphere* **14**, 3537–3550 (2020).
- 242 11. Glen, J. Experiments on the deformation of ice. *Journal of Glaciology* **2**, 111–114 (1952).
- 243 12. Nye, J. F. The distribution of stress and velocity in glaciers and ice-sheets. *Proceedings of the Royal Society of*
244 *London. Series A. Mathematical and Physical Sciences* **239**, 113–133 (1957).
- 245 13. Haefeli, R. Contribution to the movement and the form of ice sheets in the Arctic and Antarctic. *Journal of*
246 *Glaciology* **3**, 1133–1151 (1961).
- 247 14. Liboutry, L. General theory of subglacial cavitation and sliding of temperate glaciers. *Journal of Glaciology* **7**,
248 21–58 (1968).
- 249 15. Goldsby, D. & Kohlstedt, D. L. Superplastic deformation of ice: Experimental observations. *Journal of Geophysical*
250 *Research: Solid Earth* **106**, 11017–11030 (2001).
- 251 16. Ma, Y. *et al.* Enhancement factors for grounded ice and ice shelves inferred from an anisotropic ice-flow model.
252 *Journal of Glaciology* **56**, 805–812 (2010).
- 253 17. Steinemann, S. Results of preliminary experiments on the plasticity of ice crystals. *Journal of Glaciology* **2**,
254 404–416 (1954).
- 255 18. Alley, R. B. Flow-law hypotheses for ice-sheet modeling. *Journal of Glaciology* **38**, 245–256 (1992).
- 256 19. Cuffey, K. & Kavanaugh, J. How nonlinear is the creep deformation of polar ice? A new field assessment. *Geology*
257 **39**, 1027–1030 (2011).
- 258 20. Hooke, R. Flow law for polycrystalline ice in glaciers: comparison of theoretical predictions, laboratory data, and
259 field measurements. *Reviews of Geophysics* **19**, 664–672 (1981).
- 260 21. Jezek, K. C., Alley, R. B. & Thomas, R. H. Rheology of glacier ice. *Science* **227**, 1335–1337 (1985).
- 261 22. Thomas, R. H. The creep of ice shelves: interpretation of observed behaviour. *Journal of Glaciology* **12**, 55–70
262 (1973).
- 263 23. Treverrow, A., Budd, W. F., Jacka, T. H. & Warner, R. C. The tertiary creep of polycrystalline ice: experimental
264 evidence for stress-dependent levels of strain-rate enhancement. *Journal of Glaciology* **58**, 301–314 (2012).
- 265 24. Weertman, J. Deformation of floating ice shelves. *Journal of glaciology* **3**, 38–42 (1957).
- 266 25. Weertman, J. Creep deformation of ice. *Annual Review of Earth and Planetary Sciences* **11**, 215–240 (1983).
- 267 26. Bons, P. D. *et al.* Greenland Ice Sheet: Higher nonlinearity of ice flow significantly reduces estimated basal motion.
268 *Geophysical Research Letters* **45**, 6542–6548 (2018).
- 269 27. Durham, W., Heard, H. & Kirby, S. H. Experimental deformation of polycrystalline H₂O ice at high pressure and
270 low temperature: Preliminary results. *Journal of Geophysical Research: Solid Earth* **88**, B377–B392 (1983).
- 271 28. Qi, C. & Goldsby, D. L. An experimental investigation of the effect of grain size on “dislocation creep” of ice.
272 *Journal of Geophysical Research: Solid Earth* **126**, e2021JB021824 (2021).

- 273 29. Budd, W. & Jacka, T. A review of ice rheology for ice sheet modelling. *Cold Regions Science and Technology* **16**,
274 107–144 (1989).
- 275 30. Thomas, R. H. The creep of ice shelves theory. *Journal of Glaciology* **12**, 45–53 (1973).
- 276 31. Morlighem, M. *et al.* Deep glacial troughs and stabilizing ridges unveiled beneath the margins of the Antarctic ice
277 sheet. *Nature Geoscience* **13**, 132–137 (2020).
- 278 32. Gardner, A. S. *et al.* Increased West Antarctic and unchanged East Antarctic ice discharge over the last 7 years.
279 *The Cryosphere* **12**, 521–547 (2018).
- 280 33. Savitzky, A. & Golay, M. J. Smoothing and differentiation of data by simplified least squares procedures. *Analytical*
281 *chemistry* **36**, 1627–1639 (1964).
- 282 34. Diaconis, P. & Efron, B. Computer-intensive methods in statistics. *Scientific American* **248**, 116–131 (1983).
- 283 35. Goldsby, D. L. Superplastic flow of ice relevant to glacier and ice-sheet mechanics. *Glacier science and environ-*
284 *mental change*, 308–314 (2006).
- 285 36. Gillet-Chaulet, F., Hindmarsh, R. C. A., Corr, H. F. J., King, E. C. & Jenkins, A. In-situ quantification of ice
286 rheology and direct measurement of the Raymond Effect at Summit, Greenland using a phase-sensitive radar.
287 *Geophysical Research Letters* **38** (2011).
- 288 37. Pritchard, H. *et al.* Antarctic ice-sheet loss driven by basal melting of ice shelves. *Nature* **484**, 502–505 (2012).
- 289 38. Baker, R. W. The influence of ice-crystal size on creep. *Journal of Glaciology* **21**, 485–500 (1978).
- 290 39. Ranganathan, M., Minchew, B. M., Meyer, C. R. & Pec, M. Recrystallization of ice enhances creep and the
291 vulnerability to fracture of ice shelves. *Earth and Planetary Science Letters* **576** (2021).
- 292 40. Cuffey, K. M. & Paterson, W. S. B. *The Physics of Glaciers* (Academic Press, 2010).
- 293 41. Pegler, S. S. & Worster, M. G. Dynamics of a viscous layer flowing radially over an inviscid ocean. *Journal of*
294 *fluid mechanics* **696**, 152–174 (2012).
- 295 42. Budd, W. Ice flow over bedrock perturbations. *Journal of Glaciology* **9**, 29–48 (1970).
- 296 43. MacAyeal, D. R. in *Dynamics of the West Antarctic ice sheet* 141–160 (Springer, 1987).
- 297 44. Pegler, S. S. The dynamics of confined extensional flows. *Journal of Fluid Mechanics* **804**, 24–57 (2016).

298 Acknowledgments

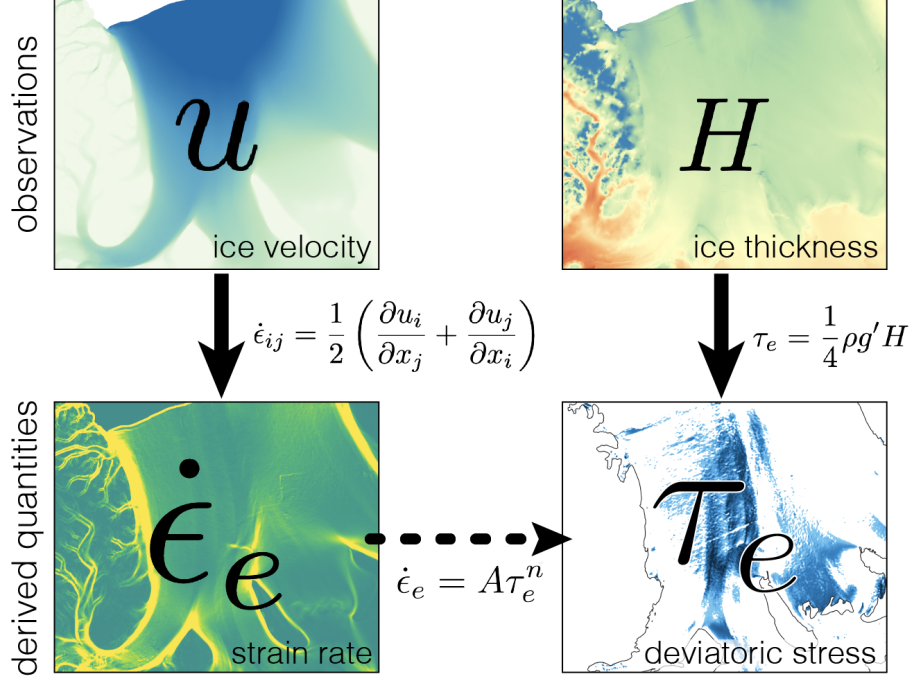
299 The authors benefited from discussions with Jerome Neufeld, Colin Meyer, and Andrew Ashton. We appreciate
300 insightful reviews from Jeremy Bassis and Paul Bons. J.D.M was partially funded through an NSF Graduate Research
301 Fellowship. J.D.M and B.M.M. were partially funded through NSF-NERC award 1853918. B.M.M. received additional
302 funding through NSF-NERC award 1739031.

303 Author contributions

304 The authors worked together to conceive and design the project. J.D.M. undertook the analysis, generated the figures,
305 and wrote the initial version of the manuscript. B.M.M. and S.S.P. helped revise the manuscript.

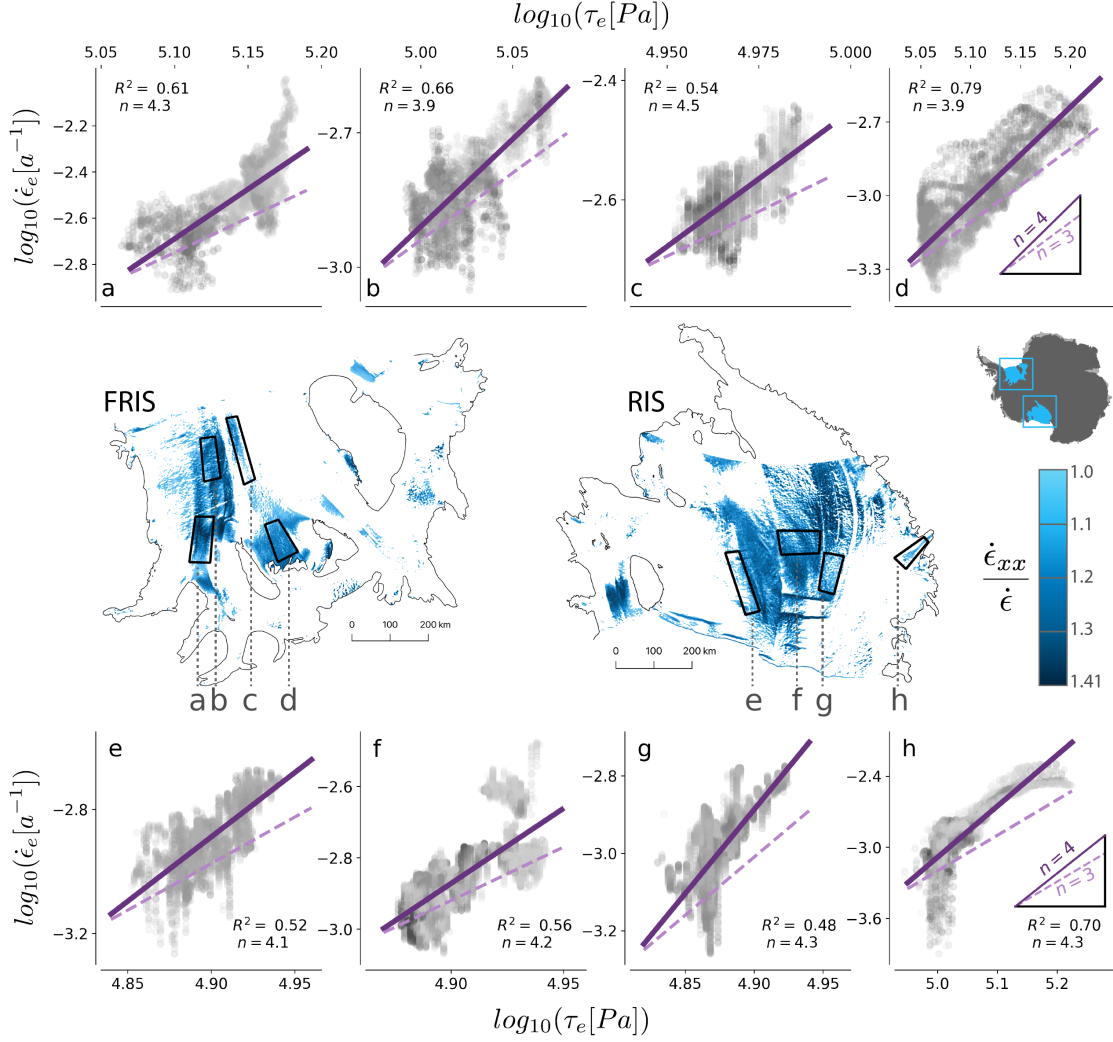
306 Competing interests

307 The authors declare no competing interests.



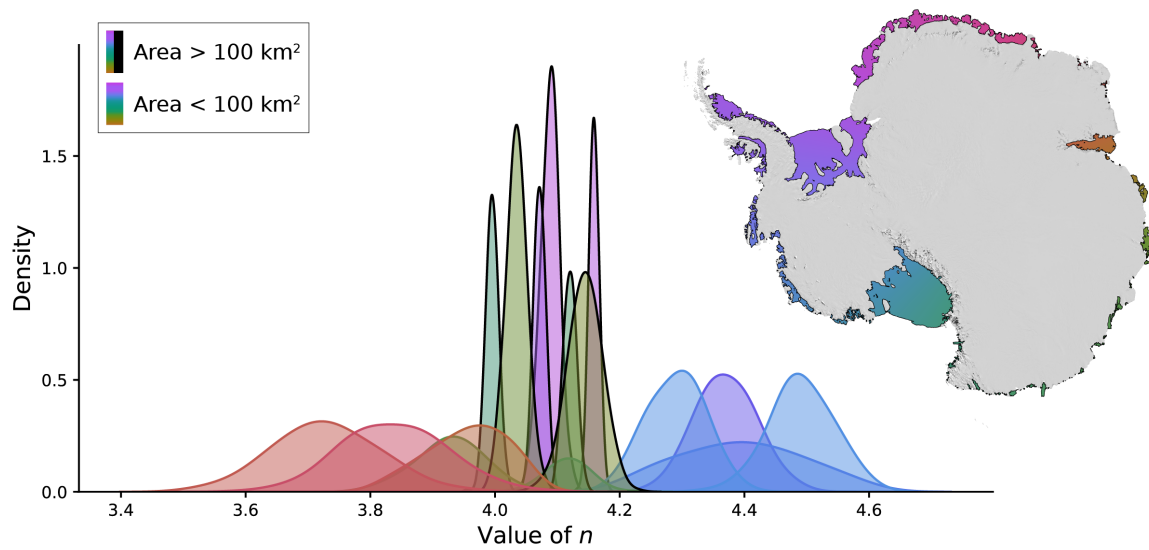
The premise of this study applied to validate and calibrate the flow law of glacier ice

Figure 1: Visual summary of our methodology. The schematic shows how we begin with publicly available satellite observations of surface velocity vector u_i and ice thickness H . Using the strain rate tensor, $\dot{\epsilon}_{ij}$, we calculate the effective strain rate $\dot{\epsilon}_e = \sqrt{\dot{\epsilon}_{ij}\dot{\epsilon}_{ij}/2}$ and along-flow strain rate $\dot{\epsilon}_{xx}$. In our areas of interest, where $\dot{\epsilon}_{xx} \approx \dot{\epsilon}_e$, we estimate the effective deviatoric stress $\tau_e = \sqrt{\tau_{ij}\tau_{ij}/2} \approx \tau_{xx}$ using the force balance detailed in the Methods, which gives $\tau_{xx} \propto H$ (Eq. 2). The values of $\dot{\epsilon}_e$ and τ_e are then correlated through a flow law, indicated by the horizontal dashed arrow labeled with Glen's Flow Law (Eq. 1).



Regression analysis produces line of best fit corresponding to the value of the stress exponent, n

Figure 2: Estimates of effective deviatoric stress τ_e plotted against effective strain rate $\dot{\epsilon}_e$ shown as log-log plots in panels a-h, corresponding to geographic regions on Filchner-Ronne Ice Shelf (FRIS) and Ross Ice Shelf (RIS). The results of each regression substantiate a power law rheology in the form of Glen's Flow Law, where the value of n is the slope of the plotted solid line and $\log_{10}(A)$ is given by the value of the y -intercept. The color map corresponds to the value of the ratio $\dot{\epsilon}_{xx}/\dot{\epsilon}$ where a maximum value of $\sqrt{2}$ signifies a purely extensional flow regime. The range of stresses used in this plot span 65 – 165 kPa, and the range of strain rates spans 0.001–0.004 yr^{-1} . The dashed line corresponds to a slope $n = 3$ with an unrealistic value of A in order to visually match the starting point of the line segment for $n = 4$. For a comparison with existing flow laws ($n = 3$) see Supplementary Figure S3.



Inferred values of the stress exponent, n , across Antarctic ice shelves

Figure 3: Normalized kernel density estimation of the value of the stress exponent n obtained over viable regions of Antarctic ice shelves from bootstrap error estimation. The probability density shows that the value of n is concentrated at 4.1 ± 0.4 . The estimates here represent stress estimates of 50–180 kPa and effective strain rate estimates of $0.001\text{--}0.006 \text{ yr}^{-1}$ (Supplement Figure S6). Larger areas sampled from Ross Ice Shelf and Filchner-Ronne Ice Shelves show a greater range of stresses (and strain rates) and smaller spread of inferred n values in comparison to smaller geographic areas which have a narrower range of stresses and produce a greater spread in the possible values of n .